AN EXPERIMENTAL EVALUATION OF THE ROLE OF WATER VAPOR AND COLLISIONAL ENERGY ON ASH AGGREGATION IN EXPLOSIVE VOLCANIC ERUPTIONS

A Thesis
Presented to
The Academic Faculty

by

Jennifer Whitney Telling

In Partial Fulfillment
of the Requirements for the Degree
Master of Science in the
School of Earth and Atmospheric Sciences

Georgia Institute of Technology
May 2011

AN EXPERIMENTAL EVALUATION OF THE ROLE OF WATER VAPOR AND COLLISIONAL ENERGY ON ASH AGGREGATION IN EXPLOSIVE VOLCANIC ERUPTIONS

Approved by:

Dr. Josef Dufek, Advisor
School of Earth and Atmospheric Sciences
Georgia Institute of Technology

Dr. Andrew Newman
School of Earth and Atmospheric Sciences
Georgia Institute of Technology

Dr. Athanasios Nenes
School of Earth and Atmospheric Sciences
Georgia Institute of Technology

Date Approved: March 28, 2011

For my Mom and Dad

ACKNOWLEDGEMENTS

I would like to thank my friends, family and God for always giving me a reason to smile and the strength to get back up and try again. I would also like to thank my advisor, Dr. Joe Dufek, and my lab members, particularly Cindy Young, for their support and encouragement.

TABLE OF CONTENTS

LIST OF TABLES

LIST OF FIGURES

LIST OF SYMBOLS AND ABBREVIATIONS

1, 2	Particle identifier
dt	Image time step (s)
E	Collision kinetic energy (CKE) (J)
E_s	Surface energy (J)
i	x, y component
m	Particle mass (kg)
m’	Reduced mass (kg)
n	Image index number
p	Mass ratio
q	Stokes number analysis constant
r	Particle radius (m)
r’	Reduced radius (m)
s	Particle location constant
St_{cr}	Critical Stokes number
St_x	Particle Stokes number
t_i	Particle interaction time (s)
u, v	Velocity component (m/s)
w	Approach velocity (m/s)
x	Physical coordinate (m)
ε	Aggregation efficiency
μ	Viscosity (Pa·s)
τ_i	Interaction time (s)
τ_r	Rebound time (s)

SUMMARY

Eruption dynamics are sensitive to ash aggregation, and ash aggregates (e.g. accretionary lapilli) are commonly found in eruptive deposits, yet few experiments have been conducted on aggregation phenomena using natural materials. Experiments were developed to produce a probabilistic relationship for the efficiency of ash aggregation with respect to particle size, collision kinetic energy and atmospheric water vapor. The laboratory experiments were carried out in an enclosed tank designed to allow for the control of atmospheric water vapor. A synthetic ash proxy, ballotini, and ash from the 2006 eruption of Tungurahua, in Ecuador, were examined for their aggregation potential. Image data was recorded with a high speed camera and post-processed to determine the number of collisions, energy of collisions and probability of aggregation. Aggregation efficiency was dominantly controlled by collision kinetic energy and little to no dependence on atmospheric water vapor was seen in the range of relative humidity conditions tested, 20 to 80%. Equations governing the relationships between aggregation efficiency and collision kinetic energy and the related particle Stokes number, respectively, were determined for implementation into large scale numerical volcanic models.

CHAPTER 1

INTRODUCTION

Explosive volcanic plumes can reach the stratosphere and are capable of moving volcanic ash hundreds of kilometers away from its source, creating a widespread hazard (Prata and Tupper, 2009; Robock, 2000; Niemeier et al., 2009). The horizontal distribution of the plume depends on the rate of ash fallout and the wind field in the ambient atmosphere (Textor et al., 2006a; Barsotti and Neri, 2008; Schumacher and Schmincke, 1995). As the plume evolves, collisions between ash particles can produce aggregates (Gilbert and Lane, 1994; Schumacher and Schmincke, 1995). Aggregation, the adhesion of ash, can significantly reduce the transport distances of ash and can modify the dynamics of the plume (Veitch and Woods, 2001; Textor et al., 2006b). Aggregation is not confined to volcanic plumes; it also occurs in several other regions during explosive volcanism, including near-vent volcanic columns and pyroclastic density currents (Brown et al., 2010). In order to improve our understanding of particle-laden eruptive flows and the hazard models used to predict the aftermath of volcanic eruptions, it is necessary to improve our understanding of the processes driving ash aggregation (Scollo et al., 2008; Veitch and Woods, 2001; Costa et al., 2010).

Ash aggregates have been broadly defined as any conglomerate of ash particles (Gilbert and Lane, 1994). Aggregates can be formed through turbulent mixing or gravity-driven differential acceleration, with or without the presence of moisture (Schumacher and Schmincke, 1995; Gilbert and Lane, 1994). Electrostatic aggregation of solid particles and droplet coalescence of fluid drops act as end-member proxies in the study of particle aggregation. Dry charged particles can aggregate through electrostatic

attraction. This process does not require two particles to collide but only to pass within a small distance of one another; typically less than three particle diameters based on the charge density predicted for 100 μm particles (Gilbert and Lane, 1994). At the other end of the spectrum, droplet coalescence assumes that both colliding particles are fully wetted and the initially interacting surface is that of water, not the solid particles. This fully saturated behavior may be found at plume margins, where gasses have expanded and cooled, or in pyroclastic density currents, which have cooled through the entrainment of ambient air to reach saturation. Regardless of how an aggregate is formed, ash aggregates, being larger and heavier than individual pieces of ash, return to the surface more quickly than individual ash grains, diluting and decreasing the transport distance of a plume (Brazier et al., 1982; Veitch and Woods, 2001).

Aggregation efficiency is defined as the fraction of colliding particles that stick together, typically for timescales longer than one second (Brown et al., 2010). With this information and an estimate of collision rate the aggregation rate for a parcel of the volcanic region can be assigned. Typically only a small fraction of the colliding particles will also successfully aggregate. Aggregation efficiency, when applied to colliding water droplets, is termed coalescence efficiency because the droplets are becoming a single, larger, droplet (Beard et al., 2002).

The sensitivity of eruption dynamics has been shown with parameterized numerical models. Textor et al. (2006a, 2006b) used a numerical plume simulation, ATHAM, to test the effect of liquid water and ice hydrometeors, atmospheric humidity, hydrometeor salinity, electrostatic forces and particle porosity on aggregation efficiency. The microphysical parameterization showed aggregation efficiency of ash was found to

peak in dense ash flows and in regions where liquid water was present. ATHAM, like other numerical models, employed a proxy for ash aggregation in numerical simulations of volcanic plumes. This approach is common because of the time and expense of accounting for aggregation microphysics on a particle-by-particle basis and due to current limitations in our understanding of aggregation efficiency.

Veitch and Woods (2001) also modeled ash aggregation and compared it to field studies from the 1980 eruption of Mt. St. Helens. Field observations of the ash fallout showed ash volume to peak within 50 km of the eruption site and again between 300 and 350 km from the eruption site. Veitch and Woods (2001) ran both ash fallout models that did include aggregation and that did not include aggregation. The model that did not include any aggregation processes showed no secondary peak. However, the model that included aggregation predicted the secondary peak in ash volume to occur at 250 km. Though the secondary peak was not in the correct location it is still an improvement on the model run without any aggregation processes. The Veitch and Woods (2001) and Textor et al. (2006a, 2006b) work clearly indicates that aggregation has a distinct effect on the distribution of ash after a volcanic eruption.

Experimental studies on droplet coalescence and particle–droplet collisions provide a framework for discussing particle–particle aggregation. Coalescence efficiency depends on numerous factors including droplet sizes, mass, velocity and collision kinetic energy as summarized in Table 1 (Beard et al., 1979; Beard et al., 2002; Brazier-Smith et al., 1972; Low and List, 1982). All four studies collected data using similar techniques. Each allowed differently sized water droplets to fall and coalescence or bounce. These events were recorded on 35mm photographs and visually analyzed.

Table 1. Summary of previous coalescence efficiency studies.

Study	**Droplet Size (μm)**	**Material**	**Coalescence Efficiency**
Beard et al., 1979	81,20- pairs	water	0.370
Beard et al., 2002	55-105	water	0.950
Brazier-Smith et al., 1972	150-750	water	0.100 – 0.600
Low and List, 1982	> 200	water	0.500

All four of the studies in Table 1 agree that droplet energies at the onset of a collision event are an important factor in determining whether or not coalescence will occur. However, only Low and List (1982) calculates the energy of collision for coalescing water droplets. The collision kinetic energy (CKE), a widely used characterization of the collisional energy of two particles, of the 200 μm drops is, at most, 5×10^{-7} J. CKE is calculated using the reduced radius and approach velocity of the colliding particles. Beard et al. (2001) conducted studies of droplet–droplet collisions and found that coalescence tends to happen more frequently at lower particle energies (Eq. 1) whereas, at higher energies, droplets are more likely to fully rebound or to coalesce briefly and then break up.

$$\varepsilon = 0.767 - 10.14\left(\left(E/E_s\right)\cdot\left(\tau_i/\tau_r\right)\cdot\left(r_1/r_2\right)^3\right) \qquad (1)$$

where ε is the coalescence efficiency, E is the collision kinetic energy, E_s is the droplet surface energy, r_1 and r_2 are the droplet radii and τ_i and τ_r are the interaction and rebound times, respectively.

The aggregation of wet particles is physically different from droplet coalescence, especially in the case of porous and irregularly shaped ash which can accumulate water without developing a full surface coating, and experiments, beyond those conducted on

droplet pairs, need to be conducted to better model their behavior. Particle aggregation is sensitive to the surface properties of the particles. Lathem et al. (2011) showed that ash is hygroscopic and highly reactive at its surface, making it a strong candidate for water adsorption. Gilbert and Lane (1994) found that increased porosity and chemical interactions at the ash surface increase aggregation efficiency. Increased porosity led to an increased surface area for the deposition of salts and other chemical interactions. Salts, in particular, were found to act as a bonding agent for aggregates once the ash cooled enough to precipitate them out of solution (Gilbert and Lane, 1994). Each of these studies provides evidence necessary for creating a picture of what processes are important at the particle scale. However, none of them provide a direct relationship between surface processes and aggregation efficiency.

Volcanic hazard models to date have either neglected to consider ash aggregation or used a generalized proxy, often based on droplet coalescence research (Textor et al., 2006a; Barsotti et al., 2008). However, the unique composition and origin of ash, as well as the setting in which it is found, necessitate the modeling of ash as a unique species. The aim of this study is to determine probabilistic relationships between atmospheric conditions, particle energies and aggregation efficiency. Numerical simulations of these factors are costly and complex, and in situ measurements are challenging and hazardous in volcanic settings. However, in a laboratory setting, it is possible to observe the results of particle–particle collisions and determine these relationships experimentally. Experiments were designed to collect data on thousands of particle collisions and their outcomes in order to produce a measure of aggregation efficiency that can be implemented into large scale numerical models. The experiments presented here provide

new relationships for ash aggregation at varying atmospheric humidity and particle energy.

CHAPTER 2

METHODS

2.1 Experimental setup

Lab experiments were designed to test the relationship between atmospheric humidity, collisional energy and the efficiency of ash aggregation. An enclosed tank, in which relative humidity could be adjusted and monitored, was built to house the experiments. Experimental samples were accelerated into the tank through a vertical nozzle and particle positions (and velocities) were determined with a Phantom MIRO-4 high-speed camera. Data analysis was completed using a particle image velocimetry method, which has been modified for the analysis of inertial and collisional particles.

The tank was constructed out of 6.4mm thick plexiglass and is 0.61m × 0.15m × 0.61m. The particle jet assembly was constructed to inject ash samples upwards into the contained tank using a pressurized gas line connected to the bottom of the assembly. A plastic planar nozzle was affixed to the top to control the direction of particle flow out of the assembly and to increase the number of collisions in the plane probed by laser illumination. A stainless steel wire mesh, number 325, was inserted into the lower piece of copper piping, forming a stage that allowed pressurized air to move upwards, accelerating the sample loaded onto the top of the mesh, but was fine enough to not allow the sample to fall downwards into the gas line. A humidifier, with a variable output control, was connected to the tank via a sealed connection, allowing for careful regulation of the humidity in the tank. An Omega OM-73 temperature and humidity gauge was attached to the inside wall of the tank so that conditions could be monitored and recorded during trials. The temperature and humidity in the tank were measured immediately

before each trial and checked at the end of every trial to verify that neither had changed during the duration of the experiment.

A Nd:YAG laser, wavelength 532 nm, output 20 mW, was situated above the tank oriented parallel to the nozzle opening at the top of the particle jet assembly. The light illuminated the 100 μm size ash so that discrete particles could be resolved during the lab trials. The beam was approximately 200 μm wide, approximately twice the width of two particles placed side to side.

A Phantom MIRO 4 high speed camera was arranged in front of the tank to capture the motion of the particles. The lens was focused on the plane of the laser light aligned with the top of the jet nozzle. The average field of view was 0.045 m x 0.044 m, with a pixel resolution of 256 x 256 pixels, and trials were conducted at speeds ranging from 1800 to 3000 frames per second. This corresponds to a spatial resolution of approximately 176 x 172 μm per pixel. The bottom of the field of view was oriented 0.4 m above the top of the particle jet in order to allow the sample to slow down and disperse. The camera recording was triggered directly prior to the triggering of the gas line into the tank so that the full motion of the particles could be captured as they moved through the field of view. Figure 1 illustrates the full experimental setup.

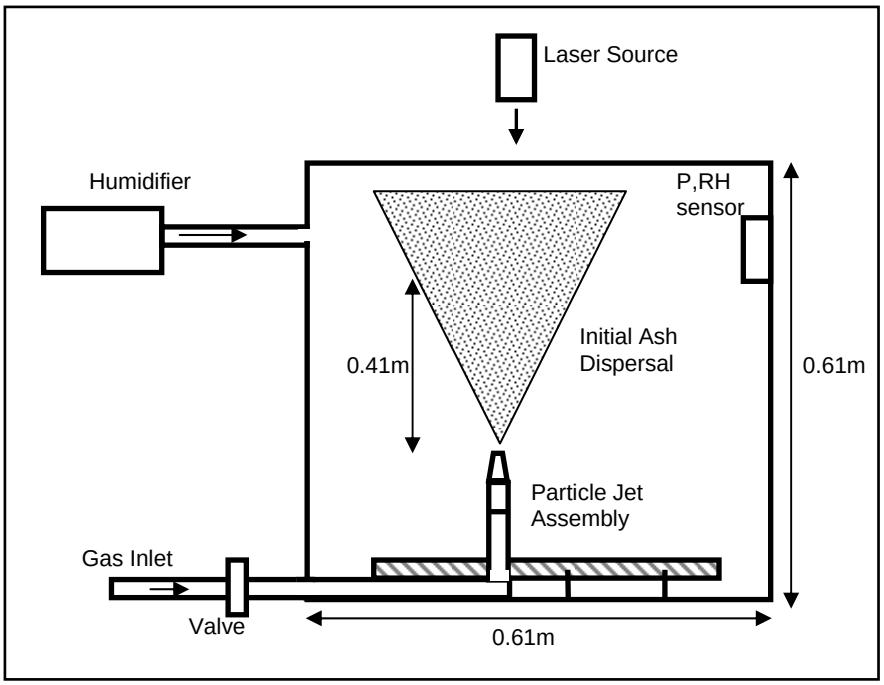

Figure 1. Diagram of the full tank setup. The camera position is not shown on this 2D rendering but would be situated directly in front of the particle jet assembly, 0.41 m above the top of the nozzle. Not to scale.

2.2 Data collection

Two different particle samples were used in the trials. The first sample was mono-disperse spherical silica with a diameter between 90-150 μm. The second sample was an ash sample collected in the field from the eruption of Tungurahua, Ecuador in 2006. Ash grains in the second sample were primarily glass fragments with some fragmented crystals. The sample was sieved to three samples with finer grain size distribution: 106 – 125 μm, 125 – 212 μm and 212 – 250 μm. The ash sample was dried on a hot plate prior to being used in the experiment to ensure that water on the sample was a product of the humidity in the tank alone.

Once a sample was loaded into the particle jet assembly and the assembly was mounted onto the stage, the tank was closed. Low humidity cases relied on the ambient relative humidity at the time of the experiment, typically 20–30%. Higher humidity trials

were run by sealing the tank and running the humidifier until the desired humidity was reached. The humidifier was then used to maintain the humidity in the tank within +/- 0.5% from the value recorded at the beginning of each trial. The temperature, relative humidity and camera recording parameters were recorded for each trial. After pressurizing the input gas line, turning off the ambient fluorescent lights and aligning the laser with the top of the jet nozzle, the particle jet and camera recording were triggered simultaneously. Each trial lasted between 30-60 seconds. Once completed, the digital files from each trial were reviewed and extracted into individual frames for analysis.

2.3 Post-processing

The images were first analyzed using an adapted form of the particle image velocimetry technique (PIV), a commonly used technique in analyzing fluid flows (Aanen, 2002). The algorithm was developed in Matlab specifically for use in these experiments because standard PIV assumes that particles follow the fluid flow field and do not interact with each other, which is not appropriate for these experiments. The algorithm tagged all of the particles in a series of images discreetly and tracked their movement by assuming that the particle in a successive image (n+1) would be closest to itself in the previous image (n). This assumption was checked by predicting each particle position out to one additional time step (n+2) and then determining whether a particle was physically present at the expected location within a tolerance factor (Figure 2). The center coordinates for each particle were determined by averaging the left and right and upper and lower bounds of each particle, for the x and y positions respectively. Matlab image analysis tools also interpolated the particle boundaries based on pixel brightness. Due to this interpolation particle positions and sizes are recorded in terms of partial or

fractional pixels. This modified PIV algorithm was used to tag and track particles that remained in the field of view over the course of four or more high-speed video frames in order to measure the energy and result of individual particle collisions. This algorithm can only measure motion and collisions occurring in the nearly 2D plane of the laser illumination. As we are only concerned with measuring the aggregation probability from numerous collisions it is not necessary to detect every collision in the 3D flow field.

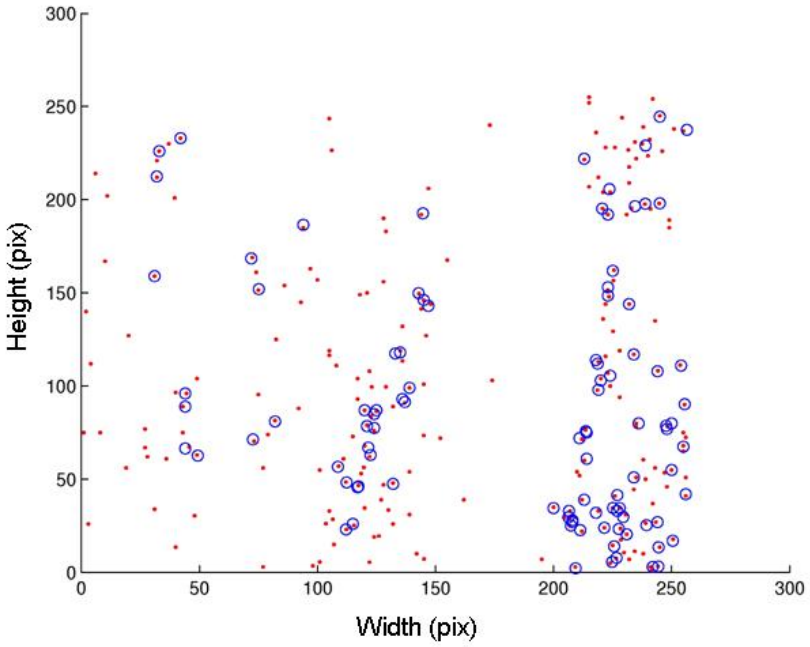

Figure 2. A computer rendering of the particle distribution in one frame of a trial with SiO_2 particles. The identified particles in the current frame are shown as red dots and the particle positions predicted from the previous frame (Eq. 2) are drawn with open blue circles. This procedure removes particles that are not moving in the plane of the laser.

Particle collisions and aggregation were analyzed based on the initial flow field data. Collisions were predicted using the velocity vectors found through PIV. Particles that were collocated in space and time were found by predicting particle locations one time step after particle velocity was determined (Eq. 2).

$$x_i^{n+2} = x_i^n + (u_i^n \cdot 2dt) \quad (2)$$

where x denotes the physical coordinate of the particle in the i dimension, u is the particle velocity and dt is the lapse time between images. The superscripts refer to the time step in a four image series. In this formulation we neglect drag over the timestep dt. The impact of drag on the particles is accounted for in the tolerance used to verify particle positions after aggregation and is discussed in more detail below. While particles were being tracked by the location of their center, each particle did have a physical size so particles did not have to be perfectly collocated in either space or time for a collision to occur. Beard et al. (2001) employed a method to solve for the period of time, t_i, in which two particles would interact (Eq. 3). The difference between the interaction time in the x and y directions had to be less than the time step between images (Eq. 4).

$$t_{i_x} = \frac{s \cdot (r_1 + r_2)}{u_1 - u_2} \text{ and } t_{i_y} = \frac{s \cdot (r_1 + r_2)}{v_1 - v_2} \quad (3)$$

$$t_i = \left| t_{i_x} - t_{i_y} \right| < dt \qquad (4)$$

where r_1 and r_2 are the two particle radii, u and v describe the velocity in the x and y dimensions and the subscripts (1 and 2) denote which particle the velocity is attributed to. The factor of s in the numerator is a dimensionless tolerance on particle proximity. Beard et al. (2001) set s equal to 2. In this analysis a tighter tolerance was used and s was set equal to 1 to counteract the effect of light scattering around particles and the possibility for particles to be recorded by more than one pixel. Either effect could make particles appear larger than they actually were. Additionally, SiO_2 particles and, to a lesser extent, some ash particles had diameters that were smaller than the physical width of a pixel,

further increasing their apparent computed size. We estimate that together these effects can increase the apparent particle size by approximately a factor of two (Figure 3).

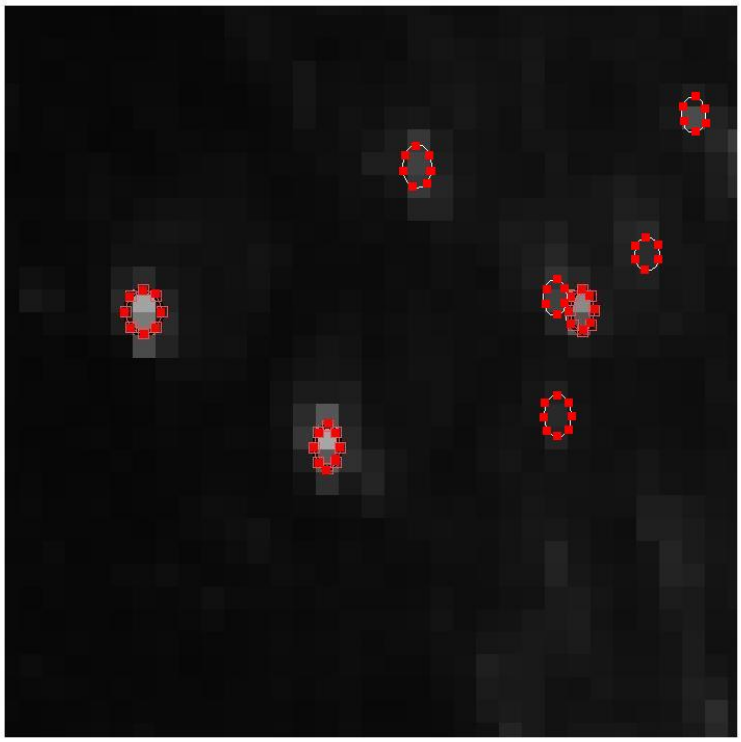

Figure 3. A raw image zoomed in to show a region 0.0042 x 0.0042 m from a SiO_2 trial. Several particles have been overlaid with their actual particle size, roughly 100 μm in diameter. The light gray pixels directly around the highlighted particles are likely the effect of light scattering while the adjacent bright pixels highlighted in at least three cases are due to particle capture across multiple pixels.

100 separate identified events were hand checked for anomalous collision identifications. The threshold value of Equation 4 was varied during the analysis to verify that the number of detected collisions decreased as the time constraint was tightened. Less than 3% of the events tested were anomalous once this value was reduced to 1/10,000. The algorithm was also tested on a set of computer generated images of particles moving through space over a series of time steps. The algorithm solved the 2D equation of motion for the particles, including drag and gravitational forces. Particles in the images

interacted with one another, bouncing or aggregating, similar to the behavior expected from physical particles. Less than 5% of the identified events from the computer generated images were false. Once a collision was detected, the involved particles were analyzed in the aggregation algorithm. Data concerning the particle sizes, velocity vectors and the result of the interaction were saved to an output file for every collision event.

To determine whether a collision resulted in an aggregation event, a simplified momentum equation (Eq. 5) for the colliding particles was solved to predict the final velocity of a possible aggregate,

$$u_i^{n+3} = \frac{(m_1 \cdot u_{i_1}^{n+2}) + (m_2 \cdot u_{i_2}^{n+2})}{m_1 + m_2} \quad . \qquad (5)$$

In this equation, m_1 and m_2 are the masses of the two particles. The final position of the aggregate was predicted, based on these velocities, for the frame following the collision event. As the momentum equation is not exact and there was some variation in the mass of the ash particles a region around the projected position was examined. A maximum value of +/- 2 pixels, in the x and y directions, was determined for the aggregation tolerance to account for the effect of gravity and drag on particle location (Raju and Meiburg, 1995; Burgisser et al., 2005). Conservatively, the algorithm required that the predicted particle position must coincide with an actual particle within +/- 1 pixel in both the x and y directions in order for the event to be considered a successful aggregation event. The solutions to over 100 positive aggregation identifications were checked manually and, of these, only 2-3% of detected events were found to be incorrect solutions. This number did not decrease significantly as the tolerance was further reduced.

Trials, at varying humidity, were run for both the silica (ballotini) and ash samples. Thirty two trials were run using the silica particulate and twenty two trials were run with the ash samples from Tungurahua, for a total of fifty four trials. The ballotini sample was primarily composed of SiO_2 (Potters Industries Inc.). The major oxide composition for the Tungurahua ash samples is from the same eruptive unit sampled by Samaniego et al. (2011). The physical parameters for these trials have been reported in Appendix A.

A bulk output file was written to summarize the run once it was complete, complementing the individual data recorded for each collision event. The file included the total number of particles in the run, the number of collision and aggregation events and the frequency of collisions (per second) averaged over the run. This bulk data, as well as the event specific data on collision and aggregation events, was used for data analysis.

CHAPTER 3

RESULTS

The effective particle size distribution for the ash and SiO_2 samples that was measured during image analysis has been reported in Figure 4. The distribution includes both aggregate and individual particles and records all frames analyzed and includes 4.2 x 10^5 SiO_2 particles and 1.8 x 10^5 ash particles. The physical size of an individual SiO_2 particle ranged from 90–150 μm. A few factors may impact the slight increase in particle size between the known distribution of sizes and the sizes measured in post-processing. Light scattering around the particles can increase the imaged size of particles, likely by no more than a factor of 1.5 to 2. Particles also might be captured by more than one pixel, enhancing their size in the high-speed images. The ash sample had a wider initial size distribution, ranging from 100–250 μm, though more trials were run with the larger ash size samples. Light scattering is less prominent for the ash sample because it is dark in color and scatters light less effectively than the white SiO_2 sample. Ash particles may also be recorded by more than one pixel, increasing their recorded size. The error resulting from particles being captured by more than one pixel was calculated in Appendix B and no more than 35% of the sample was found to be artificially enlarged. Particle diameters were used to estimate mass and momentum of particles. Particle size alone was not a conclusive metric to determine aggregation efficiency. The effects of light scattering and particle capture across multiple pixels introduced a large error to aggregation efficiency calculations performed using particle size. However, particle size dependent aggregation efficiency still provided a first order approximation of aggregation efficiency. Accounting for effects that enlarged the recorded particle sizes, SiO_2 particles

with a diameter less than 350 μm and ash particles with a diameter less than 400 μm were considered to be single particles. All larger particles were treated as aggregates. The result is a 28% aggregation efficiency for SiO_2 and a 19% aggregation efficiency for ash.

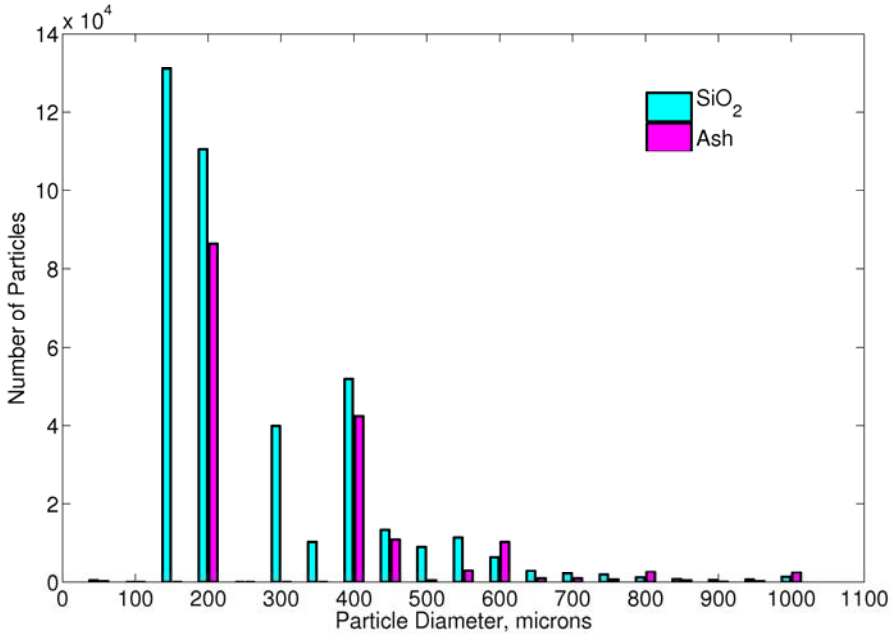

Figure 4. Particle size distribution for ash and SiO_2 samples. Effective particle diameters were measured along the longest axis of each particle for every particle identified and counted in 50 μm wide bins. Particle diameters were not altered to adjust for light scattering since the effect is not uniform across all particles. Light scattering around SiO_2 particles could increase the apparent particle diameter by approximately a factor of two times its actual size, though light scattering was not observed around every SiO_2 particle. Light scattering was less effective around ash particles due to the darker color of the volcanic ash and increased the size of these particles by a factor of less than two.

Aggregation efficiency was determined in the same way that coalescence efficiency is determined for water droplets (Glickman, 2000), as a function of the number of collisions in a given series of images, and reported as a percentage. The bulk data was averaged over ranges of 5% relative humidity. The reported error is the standard deviation for the averaged results in each bin (Figure 5). The total number of bounce and aggregations events in each bin has been reported next to the corresponding data point.

Due to the darker color of ash particulate and the blurring effect that was sometimes observed in very high humidity, RH > 70%, SiO_2 trials; no ash trials were conducted at relative humidity greater than 65%. The data exhibits little to no trend for increased aggregation with increasing relative humidity in this humidity range.

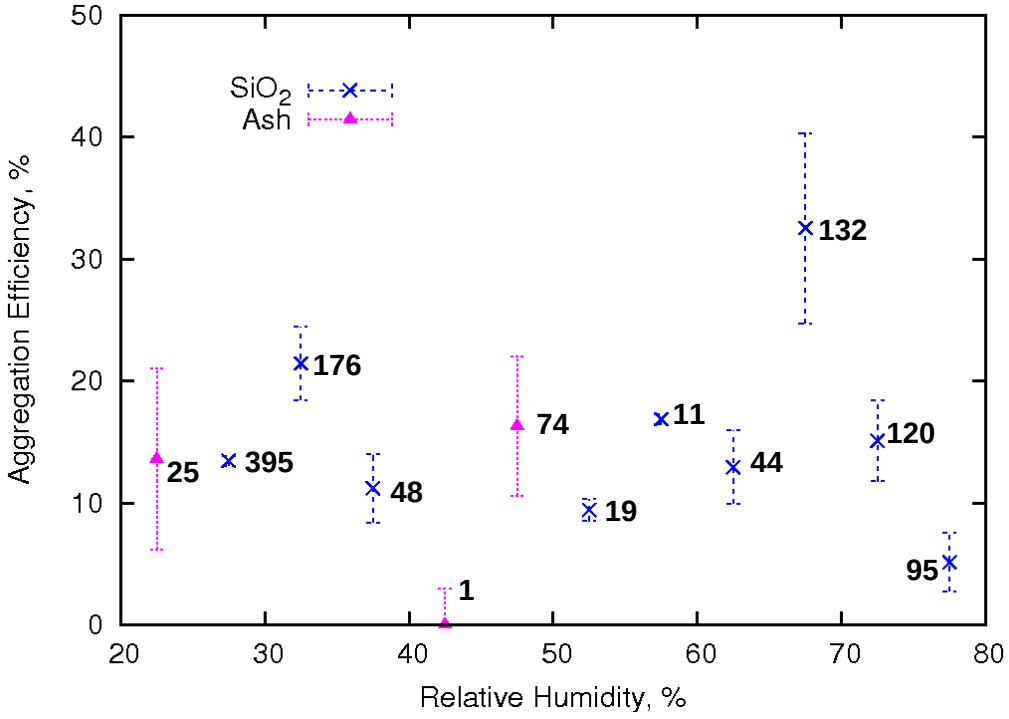

Figure 5. Aggregation efficiency as a function of relative humidity. The bin for which standard deviation could not be calculated, due to dearth of data, has a 3% error attached to it, the maximum error on the number of aggregation events calculated by hand checking bounce and aggregation solutions from the PIV algorithm. The number of data points in each bin is reported next to the bin average. Only a weak to no correlation between relative humidity and aggregation efficiency was observed.

Aggregation efficiency was also calculated for a range of CKE values (Figure 6). The technique of averaging data points within a bin was used again to handle the large quantity of data collected over fifty seven trials. CKE bins were created to maximize the number of data points per bin, minimizing the error. Each bin has a minimum of 150 SiO_2 events or 50 ash events, respectively. The maximum CKE of a SiO_2 bounce event

was 8.52 x 10^{-4} mJ and the maximum CKE of aggregation was 3.64 x 10^{-4} mJ. The difference between the maximum CKE of ash bounce, 2.80 x 10^{-4} mJ, and ash aggregation, 3.60 x 10^{-6} mJ, was much larger than that recorded for SiO_2.

Fits were applied to both the SiO_2 and ash data series (Eq. 6 and 7) with a maximum asymptotic standard error of 17%. Increasing CKE leads to a decrease in aggregation efficiency. However careful the application of these fits to the data is, it is necessary to designate an energy range in which they are applicable because the aggregation efficiency cannot become negative. Instead, aggregation efficiency becomes very low above a threshold CKE value.

$$\varepsilon_{SiO_2} = (-8.57 \cdot \log(E)) - 117.74 \text{ for CKE} \leq 1.0 \text{ x } 10^{-6} \text{ mJ} \quad (6)$$

$$\varepsilon_{ash} = (-13.57 \cdot \log(E)) - 194.43 \text{ for CKE} \leq 6.0 \text{ x } 10^{-7} \text{ mJ} \quad (7)$$

In this set of equations (Eqs. 6 and 7), ε is the aggregation efficiency and E is the CKE of a collision event.

The lack of a clear trend between relative humidity and aggregation efficiency was further tested by considering how the relationship might change with CKE. The aggregation efficiency, as a function of CKE, was determined for the SiO_2 and ash events with relative humidities between 20–50% and 50–80%. Figure 7 shows that this breakdown of aggregation efficiency is not heavily dependent on RH, even when considered jointly with CKE.

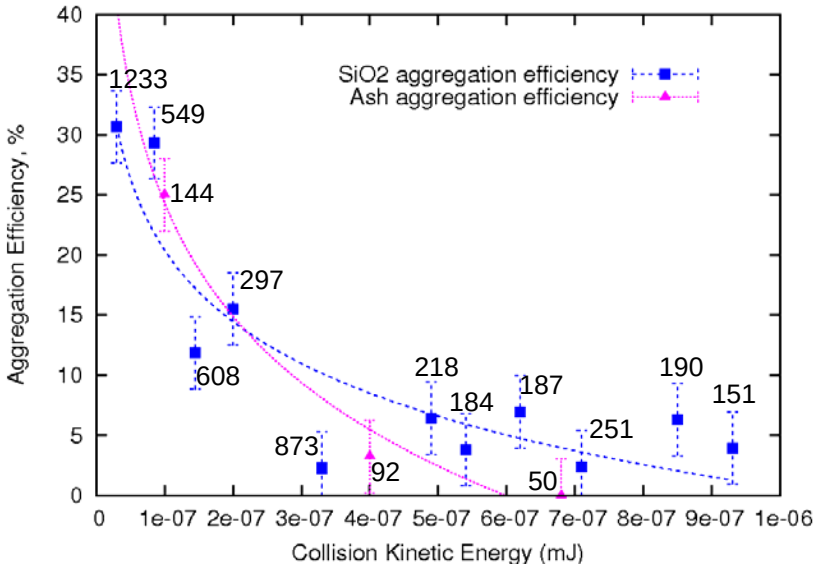

Figure 6. Aggregation efficiency as a function of CKE. Data binning along the x-axis was also utilized here however bins were created to maximize the number of events in each bin, reducing error, and are not evenly sized. Bins have at least 150 SiO_2 events or 50 ash events. The trend lines applied to the data describe the relationship between CKE and aggregation efficiency for energies below a threshold, 6 x 10^{-7} mJ for ash and 1 x 10^{-6} mJ for SiO_2. Above these values it can be assumed that the aggregation efficiency is very low but not equal to zero.

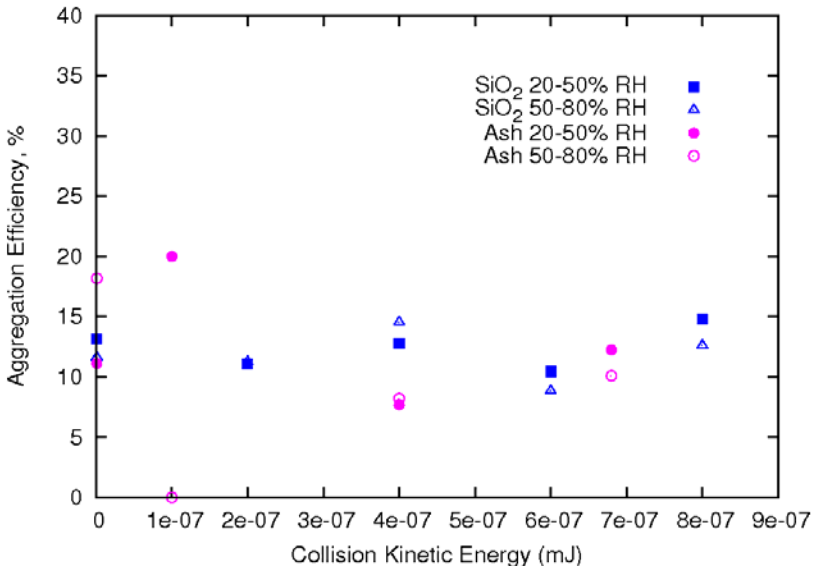

Figure 7. A plot of aggregation efficiency for both SiO_2 and ash events as a joint function of CKE and RH. There is an aggregation efficiency error of +/- 3% on each point.

CHAPTER 4

DISCUSSION

4.1 Collision and aggregation mechanisms

Electrostatic attraction and capillary forces are the two end-member cases driving aggregation events (Schumacher and Schmincke, 1995) but it is probable that both forces work to drive particle aggregation in a volcanic setting. However, individual particle charges are typically small and the distances over which they can affect a particle collision are also small, typically no more than a few particle diameters (Gilbert and Lane, 1994). Conversely, capillary forces rely on collisions between wetted particles but are orders of magnitude greater than electrostatic forces when acting to bond particles together (Schumacher and Schmincke, 1995).

4.2 Dry aggregation processes

Since no effort was made to measure particle charging in the system, the effect of electrostatic forces on the system cannot be precisely accounted for. Mechanisms for particle charging in plumes are incompletely understood but a leading theory presented by Gilbert et al. (1991) suggests that it is a result of either triboelectric charging in the plume or fracto-emission. Both mechanisms are unlikely to occur in the small scale experiments presented here. Collisional processes may still be producing charge but the size of the charges is likely quite small (Gilbert and Lane, 1994). Gilbert and Lane (1994) compare wet and dry aggregation processes and offer a method for calculating the possible effect of charging on the system. Using the estimate of particle charging presented in this work, the potential energy of two charged particles and, consequently, the CKE of two particles colliding under electrostatic forces alone, can be calculated.

Gilbert and Lane (1994) evaluated the force balance between gravitational and electrostatic forces and found that the critical distance for 100 μm scale particles was no more than three particle diameters, or 300 μm. Electrostatic attraction may increase the aggregation efficiency, above what is a product of moisture driven aggregation processes alone, but the effect is typically at least an order of magnitude smaller than the CKE for most particle collisions observed and is unlikely to inflate our aggregation efficiency considerably (Schumacher and Schmincke, 1995; Gilbert and Lane, 1994).

4.3 Wet aggregation processes

Gilbert and Lane (1994) and Beard et al. (1979, 2002) both conducted laboratory experiments on droplet aggregation. A comparison of the results of these papers to the current work has been provided in Figure 8. Gilbert and Lane (1994) also use both SiO_2 and volcanic ash samples. The experiment uses the frequency of ash uptake into a water droplet and, separately, onto a polystyrene sphere as a proxy for aggregation efficiency. A similar trend for increasing aggregation efficiency with decreasing CKE was observed. The CKE values in the Gilbert and Lane (1994) study range from 10^{-6} to 10^{-5} mJ and correspond to aggregation efficiencies of 5-11%. Compared to the results presented here, Gilbert and Lane provide an insight into the behavior of fully wetted ash collisions, which are able to produce aggregates at higher energies. The trend seen in the Gilbert and Lane data shows an asymptotic approach toward zero aggregation efficiency at high CKE that is not seen in the current data, highlighting the difference between the behaviors of ash in sub- and super-saturated flows.

In Figure 8 we compare three distinct cases in the study of wet aggregation; droplet–droplet coalescence, particle aggregation in supersaturated flows and particle

aggregation in sub-saturated flows, illustrating the importance of treating each regime separately in order to accurately model aggregation in complex multiphase flows. The Beard et al. studies used water droplets to model aggregation. Beard et al. (1979) used 20 and 81μm drops, while the Beard et al. (2002) study used larger drops, 55 to 105 μm, with a smaller difference in size, ranging up to only 25 μm between the largest and smallest drops. The later study found that aggregation efficiency increases dramatically at droplet size ratios approaching one, explaining the large difference in efficiency between the 1979 and 2002 studies. The Beard et al. (1979) study does not show the inverse relationship between aggregation efficiency and CKE seen in Gilbert and Lane (1994) as well as the current data.

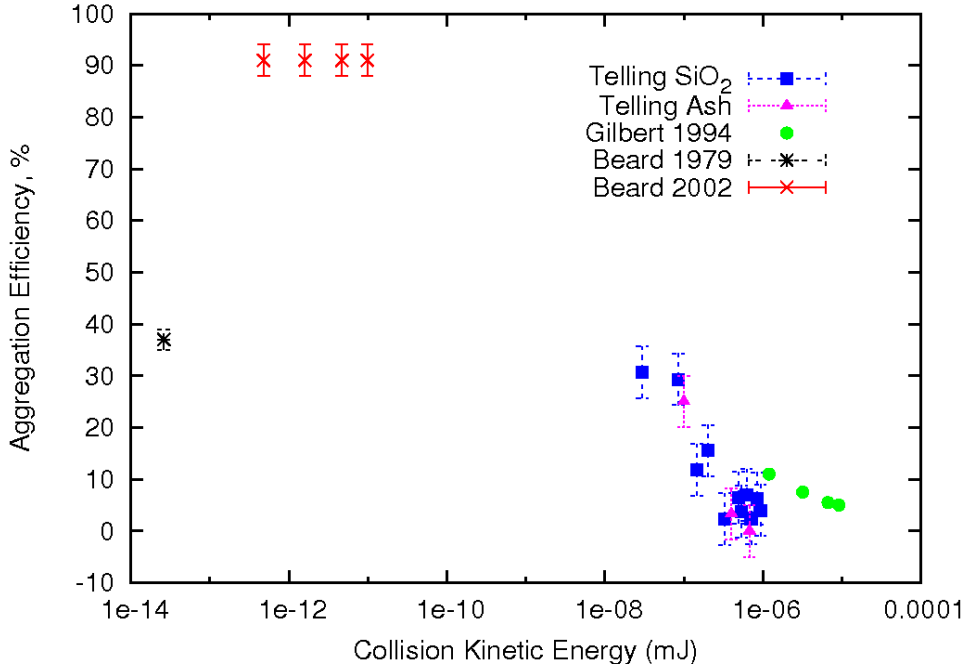

Figure 8. A comparison of previous work to the current results. Gilbert and Lane (1994) use SiO_2 traveling through a high humidity chamber while Beard et al. (1979, 2002) use water droplets only. Error data for Gilbert and Lane (1994) was unavailable.

Schmeekcle et al. (2001) considered the outward force that a thin layer of air or water will exert on two colliding particles, although at much larger particle scale than the ash particles considered here. Bounce interactions were most commonly found to be the result of high particle velocities, which produce rebound, but can also result from low particle velocities, which are unable to move particles through the layer of air or water separating the particles. Montgomery (1971) studied this behavior for the case of gravity driven collision and coalescence, estimating that collisions were most likely to result in full coalescence when droplet velocities did not exceed 50% of the terminal velocity. Orme (1997), however, also suggests that there is a lower bound on the CKE that will produce droplet coalescence. As two droplets move to collide, a layer of air between them must be moved out of the way before coalescence can take place. Low and List (1982) calculated the CKE typical to coalescence events in their experiments and found it to be on the order of $10^{-8} – 10^{-6}$ J. The CKE of aggregation events in this study was much lower, ranging from $10^{-11} – 10^{-9}$ J. Partially wetted particles, like those in this study, rebound at the higher energies expected to produce coalescence for similarly sized water droplets.

Mikhaolov et al. (2009) investigated the hygroscopicity of aerosols and found that water uptake on particles was typically accelerated above 80% relative humidity, higher than that observed in any of these experiments. Lathem et al. (2011) examined the hygroscopicity of volcanic ash and the results of their study indicate that monolayer coverage of ash should occur between 70–80%. The results of these studies necessitate more trials with ash at values of relative humidity between 50% and 90%. Schumacher and Schmincke (1995) conducted experiments on the aggregation of volcanic ash in a

fluidized bed. Aggregation increased when water accounted for 10-30 weight percent of the particles and decreased at values above or below this range. The experiments were conducted in a fluidized bed so above some threshold water filled in the interstitial volume between particles completely. Water in the flow retarded aggregation by creating an environment which more closely resembled a single phase fluid flow in which particles act as fluid tracers. Particle size and weight percent of water required for aggregation acted proportionally to each other and the smallest particles tested in the study were 300μm. Depending on the porosity of the particulate, even a very thin coating of water on the surface of a 150-200 μm ash sample would, based on the results of this study, be a likely candidate for capillary aggregation.

Volcanic flows contain large amounts of salts, particularly chloride and sulfide salts, which allow volcanic aerosols to condense before super-saturation is reached (Gilbert and Lane, 1994). However, Lathem et al. (2011) tested the hygroscopicity of seven ash samples and found six of them to correspond more closely to pure SiO_2 than to sulfate salts. The exact role that salt deposition plays in ash hygroscopicity is still not well known. Though less hygroscopic than salts, Lathem et al. (2011) showed that ash is hygroscopic and highly reactive at its surface, making it a strong candidate for water adsorption. Once salts have formed acids and condensed onto ash particles, they begin to dissolve the ash surface, which leads to increased water uptake (Delmelle et al., 2007). In the experiment presented here, the salt content is presumably much lower than that of a volcanic flow so salts cannot drive water condensation onto SiO_2 particles. Gilbert and Lane (1994) devised a way around this problem by immersing silica particles in salts and drying them before use, allowing them to produce aggregates at relative humidity values

below saturation. The surface chemistry of ash particles is permanently altered through interaction with hygroscopic compounds in volcanic flows (Rose, 1977; Delmelle et al., 2007) so the ash used in the experiments already contained hygroscopic compounds on its surface. However, little difference was seen between the behavior of SiO_2 and ash when the aggregation efficiencies were plotted against relative humidity (Fig. 5). The particles did not circulate for long in the tank and as a result only a small amount of water was condensed on particle surfaces so the primary aggregation mechanism was driven by CKE.

4.4 A cohesive model for ash aggregation

Previous work has been done using nondimensional numbers to describe the behavior of ash aggregation. A modified form of the rebound Stokes number has been derived by Schmeeckle et al. (2001) and Liu and Litster (2002). The rebound Stokes number described by this work is a ratio of the inertial force of two colliding particles divided by the hydrodynamic force of water condensed on a particle surface. Here we refer to this ratio as a rebound Stokes number to distinguish it from other usages of the term Stokes number (Raju and Meiburg, 1995). Below the critical rebound Stokes number (St_{cr}), two colliding particle will aggregate even if the only binding force is surface tension from water at the particulate surface. Above St_{cr}, colliding particles will rebound as the inertial force exceeds the hydrodynamic binding force. The critical rebound Stokes number is typically defined as a range and, within the range for a given species, collisions can result either in bounce or aggregation events, depending on other factors such as particle surface chemistry, particle charge and granular asperity, which can lead to granular interlocking. Reported values of St_{cr} vary widely. Schmeeckle et al.

(2001) defines St_{cr} as a function of particle elasticity and cites a value that can vary 39–105 for amorphous silica particles. Liu and Litster (2002) define St_{cr} as a function of the water layer thickness between two particles and particle granular asperity.

Since the granular asperity and surface water thickness were not calculated for the experiments presented here, the approach for determining rebound Stokes number presented in Schmeeckle et al. (2001) was used to analyze the results (Eq. 8).

$$St_x = \frac{8m'w^2}{3\pi\mu(2r')^2} \qquad (8)$$

where r' and m' are the reduced radius and mass of the colliding particles, μ is the viscosity of the interstitial fluid and w is the approach velocity between the two particles. The average rebound Stokes numbers for SiO_2 and ash bounce, respectively, were 269.6 and 203.0. The average rebound Stokes numbers for SiO_2 and ash aggregation were 61.9 and 34.2, well within the no-rebound range presented in Schmeeckle et al. (2001).

Costa et al. (2010) utilizes the definition of St_{cr} and the rebound Stokes number, St_x, from Liu and Litster (2002), to produce a best fit relationship between the rebound Stokes number and aggregation efficiency based on the data from Gilbert and Lane (1994),

$$\varepsilon = \frac{1}{1 + (St_x / St_{cr})^q}, \qquad (9)$$

where St_x is the rebound Stokes number of an individual collision event, St_{cr} is approximately 1.3 and q is 0.8. The same method has been used to analyze the current data in order to compare them to the results of Costa et al. (2010) (Figure 9).

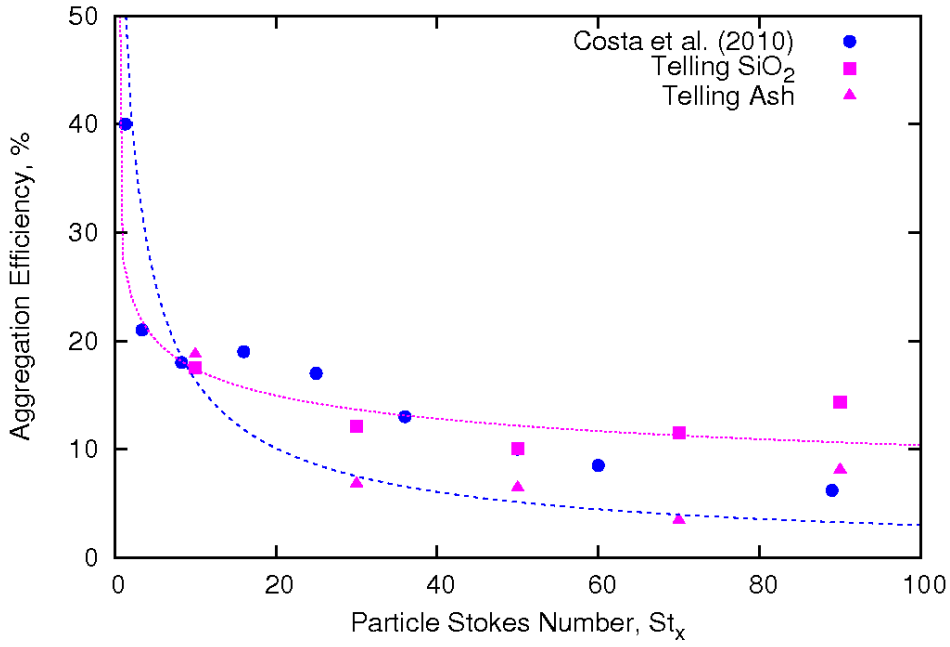

Figure 9. A comparison of the results of Costa et al. (2010) to the current data. A new fit to the data has been proposed (Eq. 10) using the St_{cr} = 40 and q=0.3, improving the fit with the results. The fit described in Costa et al. (2010) is shown in blue (Eq. 9) and the fit based on the current work is shown in purple (Eq. 10).

The current data shows that the approximation used in Costa et al. (2010) underestimates the aggregation efficiency somewhat. Based on the analysis of the rebound Stokes numbers for bounce and aggregation events, the critical rebound Stokes number is likely to fall between 35 and 200. The results of Schmeeckle et al. (2001) suggest that the value should be below 105. The best fit, with an r^2 error of roughly 8%, for the data is presented in Equation 10, where St_{cr} = 40 and q=0.26.

$$\varepsilon = \frac{1}{1+(St_x \cdot St_{cr})^q} \qquad (10)$$

Costa et al. (2010) may underestimate the efficiency of aggregation at higher rebound Stokes numbers due to the influence of aggregation mechanisms other than water driven processes. However, it is not possible to test the extent of these influences in the current

experiment. At rebound Stokes numbers less than 125, the current data shows a strong agreement with the results presented in Costa et al. (2010).

Much work has been done previously to model droplet coalescence and this proxy has been used to model particle aggregation in volcanic flows. It is likely to be a good approximation of particle behavior in supersaturated flows. More experiments need to be conducted to improve our understanding of ash aggregation at or very close to saturation. Below water vapor saturation it is still possible to form aggregates (Gilbert and Lane, 1994). By combining the current data with the results of Costa et al. (2010), a new description of ash aggregation in sub-saturated conditions has been produced. The strongest correlation with aggregation efficiency is shown through an analysis of CKE. The CKE–aggregation relationship can only be applied to collisions with a CKE less than 6.0×10^{-7} mJ. Within this range aggregation efficiency can be characterized by

$$\varepsilon_{ash} = (-13.57 \cdot \log(E)) - 194.43 \qquad (7)$$

where E is the CKE of a particle particle collision. For aggregation of rounded silica particles, aggregation efficiency may be approximated by the relationship derived for SiO_2 (Eq. 6) which has a higher threshold of 1.0×10^{-6} mJ.

$$\varepsilon_{SiO_2} = (-8.57 \cdot \log(E)) - 117.74 \qquad (6)$$

Above the threshold value, aggregation efficiency is no more than 1-2% for these conditions. Rebound Stokes number is also a useful metric for determining aggregation efficiency if sufficient information is available to calculate the critical rebound Stokes number for particles in a given flow. In this case, the threshold is determined by the particle rebound Stokes number (Eq. 8) and the critical rebound Stokes number which,

for ash particles, will typically be less than 105 (Schmeeckle et al., 2001). For sub-saturated flows

$$\varepsilon = \frac{1}{1 + (St_x \cdot 40)^{0.26}} \quad (10)$$

though more data is needed on how this relationship changes at relative humidity approaching or just above saturation, where interstitial water will dampen CKE and particles will be able to aggregate more efficiently at higher rebound Stokes numbers.

CHAPTER 5

CONCLUSIONS

Aggregation is a dynamically important process in volcanic columns. We have conducted experiments to constrain the aggregation efficiency for ash particles. The behavior of hundreds of thousands of particles, resulting in over 8,700 recorded particle interactions, was analyzed under varying relative humidity conditions to improve our understanding of particle aggregation driving mechanisms. Collision kinetic energy (CKE) and relative humidity were considered separately and CKE was found to provide a much more distinct picture of aggregation behavior in subsaturated conditions. Aggregation efficiency drops rapidly as the CKE of a specific event increases. Relative humidity also likely influences aggregation efficiency but only near saturation.

Previously, many volcanic plume models have relied on the aggregation characteristics of water droplets to model ash aggregation. A comparison of previous droplet coalescence studies to the results of Gilbert and Lane (1994), Costa et al. (2010) and the current research shows that water is a poor proxy for the behavior of ash in sub-saturated conditions. Aggregation efficiency is significantly reduced in studies of ash or ash proxies and shows a strong correlation with CKE.

Capillary, not electrostatic, forces are the most likely mechanism for bonding particles together in these experiments and can be productive even when ash is covered by only a thin or partial covering of water. Once wet aggregates have formed, ice or salt bridges can form, cementing particles to one another and increasing the probability that these aggregates will remain more cohesive than electrostatic aggregates (Textor et al., 2006b). Though relative humidity was shown to exert only a weak control on

aggregation efficiency, the importance of water in either of the primary mechanisms for wet aggregation implies that water uptake on the ash surface remains an important factor in aggregation processes.

APPENDIX A

TABLE OF PHYSICAL RUN PARAMETERS

Date	*Sample*	*Trial ID*	*Temperature, ºC*	*Relative Humidity, %*	*Width (m)*	*Height (m)*	*Spatial Resolution (µm/pix)*	*Frame Rate (per s)*	*No. of Particles*
7-Dec-09	Ballotini	1	20.6	26.3	0.036	0.038	141x148	2000	111113
		2	20.6	26.3				2000	36425
		3	21.3	73.3				2000	5698
		4	21.0	61.6				2000	51697
		5a	21.2	70.5				2000	19791
		5b	21.2	70.5				2000	14422
18-Jan-10	Ballotini	1	20.4	38.6	0.042	0.045	164x176	3000	3725
		2	20.4	38.5				3000	1358
		3	20.4	37.7				3000	622
		4	20.4	38.5				2801	3319
		5	20.5	36.7				2900	5353
		6a	20.6	54.6				2900	8798
		6b	20.6	54.6				2900	10088
		7	20.6	59.0				2900	12742
		8	20.5	59.9				2900	31633
		9a	20.5	65.9				2900	12353
		9b	20.5	65.9				2900	23571
		10	20.6	75.3				2900	8224
25-Jan-10	Ballotini	1a	19.6	34.1	0.045	0.044	176x172	2000	1943
		1b	19.6	34.1				2000	1943
		3a	19.7	31.5				2801	4140
		3b	19.7	31.5				2801	2344

Date	*Sample*	*Trial ID*	*Temperature, ºC*	*Relative Humidity, %*	*Width (m)*	*Height (m)*	*Spatial Resolution (µm/pix)*	*Frame Rate (per s)*	*No. of Particles*
25-Jan-10		4	20.2	66.1				2801	6520
		5a	20.1	66.2				2900	3697
		5b	20.1	66.2				2900	3407
		6	20.1	66.8				2900	1447
		7	20.1	72.4				2900	1500
		8	20.1	74.3				3000	2258
		9a	20.1	75.7				2900	6637
		9b	20.1	75.7				2900	17312
		10a	20.1	70.3				2900	3087
		10b	20.1	70.3				2900	5889
1-Feb-10	Ash	3a	20.9	23.1	0.045	0.044	176x172	1800	864
		3b	20.9	23.1				1800	1517
		4b	21.0	23.2				1800	1418
		5b	21.0	23.5				1800	2376
		6b	21.1	23.6				1800	2634
		7	21.1	23.8				1800	809
		8b	21.4	47.2				1800	1697
		9	21.6	53.7				1800	3443
3-Feb-10	Ash	2a	20.4	25.7	0.045	0.044	176x172	2400	3092
		3a	20.5	26.4				2200	1604
		4a	20.6	26.3				2000	9184
		5a	21.2	59.5				2000	1791
		6a	21.2	62.8				1800	9347
		6b	21.2	62.8				1800	29348
		6c	21.2	62.8				1800	20239
		6d	21.2	62.8				1800	14758
		7b	21.1	64.5				1800	17477
		7c	21.1	64.5				1800	10860
		8a	21.0	62.1				1800	5582

Date	*Sample*	*Trial ID*	*Temperature, ºC*	*Relative Humidity, %*	*Width (m)*	*Height (m)*	*Spatial Resolution (µm/pix)*	*Frame Rate (per s)*	*No. of Particles*
3-Feb-10		8b	21.0	62.1				1800	19701
		8c	21.0	62.1				1800	21688
22-Feb-10	Ash	5	20.9	43.5	0.045	0.044	176x172	2000	2062

APPENDIX B

ERROR CALCULATION FOR PARTICLE SIZE DISTRIBUTION

The statistical error produced from single particles being captured by more than one pixel was calculated using the SiO_2 sample. A uniform particle size distribution was assumed initially. The original color images were converted to black and white when the files were imported to Matlab. In order for a pixel to be interpreted as containing data, 10% of the pixel must be occupied by a particle. This tolerance was set manually.

A rectangular area within each pixel can be created so that a particle center contained within the area will take up less than 10% of any adjacent pixel (Figure B1). If the particle center falls outside the rectangle then at least 10% of it will be in an adjacent pixel. The size of the rectangle depends on the particle size.

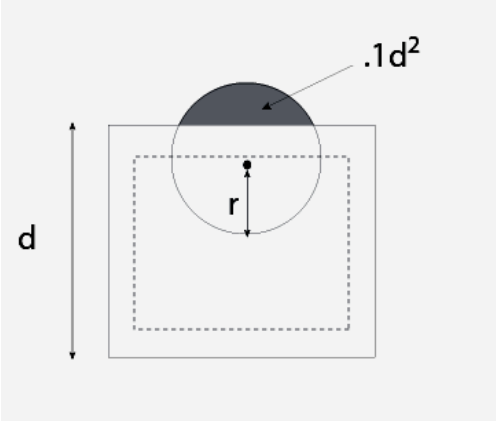

Figure B1. A single pixel (solid line) contains a rectangle (dashed line) and a particle with its center just at the boundary so that 10% of the particle is present in the adjacent pixel.

This situation can be expressed mathematically as

$$2\int_{l}^{r} r\sqrt{1-\frac{x^2}{r^2}}\,dx > .1d^2 \qquad \text{(B1)}$$

and, when integrated, the equation becomes

$$\frac{\pi}{2}r^2 - rl\sqrt{1-\frac{l^2}{r^2}} + r\sin^{-1}\left(\frac{l}{r}\right) > .1d^2 \quad , \qquad \text{(B2)}$$

where l is the distance between the edge of the rectangle and the edge of the pixel. To consider the results from this expression, the resultant particle sizes were binned using the same bins as in Figure 4. Only 35% of the particles are enlarged enough to fall outside their anticipated size range so it can be concluded that no more than 35% of the population reported in Figure 4 has been artificially enlarged due to multiple pixel capture of single particles.

REFERENCES

Aanen, L., 2002. "Measurements of turbulent scalar mixing by means of a combination of PIV and LIF." Delft University Press, Netherlands.

Barsotti, S., Neri, A., and Scire,J., 2008. "The VOL-CALPUFF model for atmospheric ash dispersal: 1. Approach and physical formulation." Journal of Geophysical Research, 113:BO3208.

Beard, K.V., Ochs, H.T., and Tung, T.S., 1979. "A measurement of the efficiency for collection between cloud drops." Journal of the Atmospheric Sciences, 36:2478-2483.

Beard, K.V., Ochs, H.T., and Liu, S., 2001. "Collisions between small precipitation drops. Part III: Laboratory measurements at reduced pressure." Journal of the Atmospheric Sciences, 58:1395-1408.

Beard, K.V., Durkee, R.I., and Ochs, H.T., 2002. "Coalescence efficiency measurements for minimally charged cloud drops." Journal of the Atmospheric Sciences, 59:233-243.

Brazier, S., Davis, A., Sigurdsson, H. and Sparks, R., 1982. "Fall-out and deposition of volcanic ash during the 1979 explosive eruption of the Soufriere of St. Vincent." Journal of Volcanology and Geothermal Research, 14:335-359.

Brazier-Smith, P.R., Jennings, S.G. and Latham, J., 1972. "The interaction of falling water drops: coalescence." Proc. R. Soc. London, 326:393-408.

Brown, R., Branney, M., Maher, C. and Davila-Harris, P., 2010. "Origin of accretionary lapilli within ground-hugging density currents: Evidence from pyroclastic couplets on Tenerife." Geological Society of America Bulletin, 122:305-320.

Burgisser, A., Bergantz, G. and Breidenthal, R., 2005. "Addressing complexity in laboratory experiments: the scaling of dilute multiphase flows in magmatic systems." Journal of Volcanology and Geothermal Research, 141:245-265.

Costa, A., Filch. and Macedonia., 2010. "A model for wet aggregation of ash particles in volcanic plumes and clouds: Theoretical formulation." J. Geophys.Res.,115, B09201.

Delmelle, P., M. Lambert, Y. Dufrene, P. Gerin, and N. Oskarsson (2007), Gas/aerosol - ash interaction in volcanic plumes: New insights from surface analyses of _ne ash particles, Earth and Planetary Science Letters, *259*, 159-170.

Gilbert, J.S., Lane, S., Sparks, R., and Koyaguchi, T., 1991. "Charge measurements on particle fallout from a volcanic plume." Nature, 349:598-600.

Gilbert, J.S. and Lane, S.J., 1994. "The origin of accretionary lapilli." Bulletin of Volcanology, 56:398-411.

Glickman, T., 2000. American Meteorological Association: Glossary of Meteorology. Second Edition. American Meteorological Association, Cambridge, MA.

Lathem, T., Kumar, P., Nenes, A., Dufek, J., Sokolik, I., Trail, M., Russell, A. and Clarke, A., 2011. "The Hygroscopic properties of volcanic ash." Geophysical Research Letters, In Review.

Liu, L.X. and Litster, J.D., 2002. "Population balance modeling of granulation with a physically based coalescence kernel." Chem.Eng.Sci., 57:2183-2191.

Low, T.B. and List, R., 1982. "Collision, coalescence and breakup of raindrops. Part I: Experimentally established coalescence efficiencies and fragment size distributions in breakup." Journal of Atmospheric Sciences, 39:1591-1606.

Mikhailov, E., Vlasenko, S., Martin, S., Koop, T. and Poschl, U., 2009. "Amorphous and crystalline aerosol particles interacting with water vapor: conceptual framework and experimental evidence for restructuring, phase transitions and kinetic limitations." Atmos. Chem. Phys., 9:9491-9522.

Montgomery, D.N., 1971. "Collision and coalescence of water droplets." Journal of Atmospheric Sciences, 28:292-293.

Neimeier, U., Timmreck, C., Graf, H., Kinne, S., Rast, S. and Self, S., 2009. "Initial fate of fine ash and sulfur from large volcanic eruptions." Atmospheric Chemistry and Physics Discussions, 9:17531-17577.

Orme, M., 1997. "Experiments on droplet collisions, bounce, coalescence and disruption." Prog. Energy Combust. Science, 23:65-79.

Prata, A.J. and Tupper, A., 2009. "Aviation hazards from volcanoes: the state of the science." Natural Hazards, 51:239-244.

Raju, N. and Meiburg, E., 1995. "The accumulation and dispersion of heavy particles in forced two-dimensional mixing layers. Part 2: The effect of gravity." Phys. Fluids, 7:1241-1264.

Robock, A., 2000. “Volcanic eruptions and climate.” Reviews of Geophysics, 38:191-219.

Rose, W., 1977. “Scavenging of volcanic aerosol by ash: Atmospheric and volcanologic implications.” Geology, 5:621-624.

Samaniego, P., Le Pennac, J., Robin, C. and Hidalgo, S., 2011. “Petrological analysis of the pre-eruptive magmatic process prior to the 2006 explosive eruptions at Tungurahua volcano (Ecuador).” Journal of Volcanology and Geothermal Research, 199:69-84.

Schmeekle, M., Nelson, J., Pitlick, J. and Bennett, J., 2001. “Interparticle collision of natural sediment grains in water.” Water Resources Research, 37:2377-2391.

Schumacher, R. and Schminke, H., 1995. “Models for the origin of accretionary lapilli.” Bulletin of Volcanology, 56:626-639.

Scollo, S., Folch, A. and Costa, A., 2008. “A parametric and comparative study of different tephra fallout models.” Journal of Volcanology and Geothermal Research, 176:199-211.

Textor, C., Graf, H., Herzog, M., Oberhuber, J., Rose, W. and Ernst, G., 2006a. “Volcanic particle aggregation in explosive eruption columns. Part I: Parameterization of the microphysics of hydrometeors and ash.” Journal of Volcanology and Geothermal Research, 150:359-377.

Textor, C., Graf, H., Herzog, M., Oberhuber, J., Rose, W. and Ernst, G., 2006b. “Volcanic particle aggregation in explosive eruption columns. Part II: Numerical experiments.” Journal of Volcanology and Geothermal Research, 150:378-394.

Veitch, G. and Woods, A.W., 2001. “Particle aggregation in volcanic eruption columns.” Journal of Geophysical Research, 106:26425-26441.